

## MIT Open Access Articles

*Study of a Model Equation in Detonation Theory*

The MIT Faculty has made this article openly available. **Please share** how this access benefits you. Your story matters.

**Citation:** Faria, Luiz M., Aslan R. Kasimov, and Rodolfo R. Rosales. "Study of a Model Equation in Detonation Theory." *SIAM Journal on Applied Mathematics* 74, no. 2 (April 24, 2014): 547–570. © 2014, Society for Industrial and Applied Mathematics.

**As Published:** <http://dx.doi.org/10.1137/130938232>

**Publisher:** Society for Industrial and Applied Mathematics

**Persistent URL:** <http://hdl.handle.net/1721.1/89464>

**Version:** Final published version: final published article, as it appeared in a journal, conference proceedings, or other formally published context

**Terms of Use:** Article is made available in accordance with the publisher's policy and may be subject to US copyright law. Please refer to the publisher's site for terms of use.



## STUDY OF A MODEL EQUATION IN DETONATION THEORY\*

LUIZ M. FARIA<sup>†</sup>, ASLAN R. KASIMOV<sup>†</sup>, AND RODOLFO R. ROSALES<sup>‡</sup>

**Abstract.** Here we analyze properties of an equation that we previously proposed to model the dynamics of unstable detonation waves [A. R. Kasimov, L. M. Faria, and R. R. Rosales, Model for shock wave chaos, *Phys. Rev. Lett.*, 110 (2013), 104104]. The equation is  $u_t + \frac{1}{2} (u^2 - uu(0^-, t))_x = f(x, u(0^-, t))$ ,  $x \leq 0$ ,  $t > 0$ . It describes a detonation shock at  $x = 0$  with the reaction zone in  $x < 0$ . We investigate the nature of the steady-state solutions of this nonlocal hyperbolic balance law, the linear stability of these solutions, and the nonlinear dynamics. We establish the existence of instability followed by a cascade of period-doubling bifurcations leading to chaos.

**Key words.** detonation instability, chaos, shock wave

**AMS subject classifications.** 35L04, 35L50, 35L67, 37N10, 76L05, 76N15, 80A32

**DOI.** 10.1137/130938232

**1. Introduction.** A detonation is a shock wave that propagates in a reactive medium where exothermic chemical reactions are ignited as a result of the heating by the shock compression. The energy released in these reactions, in turn, feeds back to the shock in the form of compression waves and thus sustains the shock motion. The dynamics of such shock-reaction coupling is highly nonlinear due to the sensitivity of the chemical reactions to temperature, making the problem significantly more challenging than shock dynamics in nonreactive media. A steady planar detonation wave is rarely observed in experiments. Complex time-dependent and multidimensional structures tend to develop [14, 26]. Numerical simulations of the equations of reactive gas dynamics are able to reproduce at a qualitative level the complex structures observed in experiments (see, e.g., [40, 1, 30]). However, obtaining physical insights into the basic mechanisms of the instability requires simplified modeling and remains challenging.

In one dimension, the instabilities of the reactive shock wave manifest themselves in the form of a “galloping detonation” [15, 14], wherein the shock speed oscillates around its steady value. It has been shown through extensive numerical experiments that as the activation energy,  $E$ , a parameter in the equations measuring the temperature sensitivity of the chemical reactions, is varied, the shock speed transitions from a constant to an oscillatory function. Further increase of  $E$  leads to a period-doubling bifurcation cascade, which ultimately results in the shock moving at a chaotic speed [29, 20]. The mechanism for such instabilities is still not completely understood.

In this paper, we show that the model introduced in [23], which consists of a single nonlocal partial differential equation (PDE), is capable of reproducing the complexity observed in one-dimensional simulations of reactive Euler equations. The model possesses traveling wave solutions precisely analogous to the ZND theory (named after Zel’dovich [44], von Neumann [41], and Döring [6], who independently developed the

---

\*Received by the editors September 23, 2013; accepted for publication (in revised form) January 24, 2014; published electronically April 24, 2014. The preprint version of this paper is posted at <http://arxiv.org/abs/1309.5080>.

<http://www.siam.org/journals/siap/74-2/93823.html>

<sup>†</sup>Applied Mathematics and Computational Sciences, KAUST, Thuwal 23955-6900, Saudi Arabia (luiz.faria@kaust.edu.sa, aslan.kasimov@kaust.edu.sa).

<sup>‡</sup>Department of Mathematics, MIT, Cambridge, MA 02139 (rrr@math.mit.edu). This author’s work was partially supported by NSF grants DMS-1115278, DMS-1007967, and DMS-0907955.

theory in the 1940s), with both the Chapman–Jouguet (CJ) case and the overdriven solutions present. Furthermore, stability analysis and unsteady simulations of the model demonstrate the complexity seen in galloping detonations, particularly their chaotic dynamics. These findings suggest that a theory much simpler than the full reactive Euler equations may be capable of describing the rich shock dynamics observed in *one-dimensional* detonation waves.

Simplified models have been used in the past to study detonations. Both rational asymptotic theories and ad hoc models have been introduced previously to gain insight into the dynamics of detonation. The reader can find extensive references in the recent review articles and books [45, 26, 5]. The most relevant to our study is the theory of weakly nonlinear detonations [32], which is a model derived asymptotically from the reactive Euler equations. Before [32], Fickett [9] and Majda [27] independently introduced ad hoc analog models, which were based on the idea of extending Burgers' equation by an additional equation modeling chemical reactions. The effect of chemical reactions in these analogs appears as a modification of the flux function to include the chemical energy term. The analog models received much attention in the past [9, 10, 11, 12, 13, 31] and continue to attract interest from a mathematical point of view [21]. These simplified models possess a theory analogous to steady ZND theory, with its CJ, strong, and weak detonation solutions. The weakly nonlinear model [32] is a result of an asymptotic reduction of the reactive Euler equations. It applies in any number of spatial dimensions, reducing in one dimension to equations very similar to those of the analogs and therefore also containing the theory of steady ZND waves. The analog models have been thought to perform poorly in describing galloping one-dimensional instabilities and the transition to chaos. However, the recent work of Radulescu and Tang [31] demonstrates that a slightly modified version of Fickett's analog, to include a two-stage chemical reaction with an inert induction zone and a following reaction zone, reproduces much of the complexity of detonations in reactive Euler equations. We suggest that even a much simpler scalar equation can capture many of the known phenomena of pulsating detonation waves.

The remainder of this paper is structured as follows. In section 2, we introduce the model and discuss its connection with the weakly nonlinear model. Next, we develop a general theory for the proposed equation and compute the possible steady ZND solutions. In section 3, we derive a dispersion relation for the linear stability and prove certain important properties about the distribution of the eigenvalues. Finally, in section 4, we focus on a specific example, for which we perform an extensive numerical study. With the example, we calculate the linear stability spectrum, the onset of instabilities, and the long-time nonlinear dynamics of solutions. Using tools from the theory of dynamical systems, we show that the solution goes through a sequence of period-doubling bifurcations to chaos, much like in the reactive Euler equations.

**2. The model.** Our model construction is based on two basic ideas: weakly nonlinear approximation [32] and nonlocality of the chemical energy release rate [10]. The precise nature of this nonlocality is explained below. The weakly nonlinear theory of detonation in one dimension, in the inviscid limit, results in the following simplified system [32]:

$$(2.1) \quad u_t + \left( \frac{u^2}{2} + \frac{q}{2} \lambda \right)_\eta = 0,$$

$$(2.2) \quad \lambda_\eta = \omega(\lambda, u),$$

where  $t$  and  $\eta$  are time and spatial variables, respectively;  $\lambda$  is the mass fraction of reaction products, going from 0 ahead of the shock to 1 in the fully burnt mixture;  $u$  can be thought of as, for example, a temperature;  $\omega(\lambda, u)$  is the reaction rate; and  $q$  is a constant representing the chemical heat release. Note that (2.2) propagates waves instantaneously since the time derivative is missing in the equation. Nevertheless, (2.1)–(2.2) constitute a hyperbolic system.

In [32], (2.1)–(2.2) are derived under the assumption of weak heat release and high activation energy. This is consistent with a weakly nonlinear theory in which (in appropriate dimensionless units) the waves and the heat release have size  $O(\epsilon)$ , while the activation energy is  $O(1/\epsilon)$ , where  $0 < \epsilon \ll 1$ .

Consider a shock moving into an unreacted ( $\lambda = 0$ ), unperturbed ( $u = 0$ ) region. At the shock, we apply the Rankine–Hugoniot conditions to (2.1) to obtain

$$(2.3) \quad -D[u] + \frac{1}{2}[u^2] + \frac{q}{2}[\lambda] = 0,$$

where  $D$  is the shock speed and the brackets denote the jump across the shock in the enclosed variables. Using  $[\lambda] = 0$  and that  $u = 0$  ahead of the shock, it follows from (2.3) that  $D = \dot{\eta}_s = u_s/2$ , where  $\eta_s(t)$  is the shock position and  $u_s = u(\eta_s^-, t)$  denotes the postshock value of  $u$ . A change of variables to the shock-attached frame, given by  $x = \eta - \eta_s(t)$ , yields

$$(2.4) \quad u_t + \left( \frac{u^2}{2} + \frac{q}{2}\lambda - Du \right)_x = 0,$$

$$(2.5) \quad \lambda_x = \omega(\lambda, u)$$

for  $x \leq 0$ , and  $u = 0$ ,  $\lambda = 0$  for  $x > 0$ .

Now we make the important assumption that  $\omega(\lambda, u) = \omega(\lambda, u_s)$ . This simplifying assumption is the reason why we call the model nonlocal, because the change of  $\lambda$  at any given point  $x$  at time  $t$  is determined not by  $u(x, t)$  at that point, but by  $u$  at the shock,  $x = 0$ . This means that any change of  $u_s(t)$  propagates instantaneously over the whole domain,  $x < 0$ . Note that such an assumption is sometimes used in modeling detonation in condensed explosives. The idea behind it is that the energy release is primarily controlled by how hard the explosive is hit by the shock [42, 10].

As a consequence of the assumed form of  $\omega$ , equation (2.5) can now be integrated over  $x$  to yield  $\lambda = F(x, u_s)$ . Upon differentiation of the latter with respect to  $x$  and substitution into (2.4) (letting  $qF_x/2 = f$ ), we obtain one nonlocal equation on the half-line,  $x \leq 0$ , given by

$$(2.6) \quad u_t + \frac{1}{2}(u^2 - uu_s)_x = f(x, u_s).$$

Conversely, it can be shown that for any positive function,  $f$ , a function  $\omega(\lambda, u_s)$  can be found such that (2.6) is equivalent to the system given by (2.4)–(2.5).

The shock, which is now located at  $x = 0$  for any  $t$ , must satisfy the Lax conditions, that is,  $c(0^-, t) > 0 > c(0^+, t)$ , where  $c = u - u_s/2$  denotes the characteristic speed in (2.6). It follows that  $D(t) = u_s/2 = c(0^-, t) > 0$ .

Initial data for (2.6) are given as  $u(x, 0) = g(x)$  for  $x < 0$ , where  $g(x)$  is a suitable function and  $u(x, 0) = 0$  for  $x > 0$  is assumed implicitly. An important feature of (2.6) is that the boundary value of the unknown,  $u_s$ , is contained within the equation. This is one of the key reasons for the observed complexity of the shock dynamics. While

the boundary information from the shock at  $x = 0$  is propagated instantaneously throughout the solution domain at  $x < 0$ , there is a finite-speed influence propagating from the reaction zone toward the shock along the characteristics of (2.6).

In characteristic form, (2.6) can be written as

$$(2.7) \quad \frac{du}{d\tau} = f(x, u_s),$$

$$(2.8) \quad \frac{dx}{d\tau} = u - \frac{u_s}{2},$$

where the characteristic speed is  $c = u - u_s/2$ . Therefore, (2.6) incorporates, within a single scalar equation, the nonlinear interaction of two waves. One is the usual Burgers wave propagating toward the shock at a finite speed,  $c$ . The other is of an unusual type, as it represents an instantaneous effect by the state  $u_s$  at the shock,  $x = 0$ , on the whole solution region  $x < 0$ . Physically, this second wave corresponds to the particle paths carrying the reaction variable, as explained in [23]. In the weakly nonlinear limit, these paths have, effectively, an infinite velocity.

**3. Steady solutions and their stability.** In this section, we explore some general properties of the proposed model. Keeping in mind the connection with detonation theory, we restrict our attention to  $f(x, u_s)$  such that  $\int_{-\infty}^0 f(x, u_s) dx = q/2 = \text{const}$ . This condition means that the amount of energy released by the reactions is finite and fixed. We consider only exothermic reactions; hence,  $f(x, u_s) \geq 0$ . Although these assumptions facilitate some of the computations, they are not required for most of the results presented here, and more general forms of the forcing can be considered without adding much more complexity to the analysis.

**3.1. Steady-state solutions.** Let  $u_0(x)$  denote a steady-state smooth solution of (2.6). It is a solution of

$$(3.1) \quad \left(u_0 - \frac{u_{0s}}{2}\right) u_0' = f(x, u_{0s}),$$

where “ $'$ ” denotes the derivative with respect to  $x$  and  $u_{0s} = u_0(0)$  is the steady-state value of  $u$  at  $x = 0$ , which is to be found together with  $u_0(x)$ . Integration of (3.1) from 0 to  $x$  yields a quadratic equation for  $u_0$ ,

$$u_0^2 - u_0 u_{0s} = 2 \int_0^x f(y, u_{0s}) dy,$$

where the integration constant vanishes in view of the boundary condition at  $x = 0$ . The solution profile is thus given by

$$(3.2) \quad u_0(x) = \frac{u_{0s}}{2} + \sqrt{\frac{u_{0s}^2}{4} + 2 \int_0^x f(y, u_{0s}) dy}.$$

The plus sign is chosen here to satisfy the boundary condition at  $x = 0$ . We note that for  $u_0(x)$  in (3.2) to be real,  $f$  must be constrained so that, at any  $x$ , the expression under the square root is nonnegative. Effectively, this is the requirement of overall exothermicity of the source term.

The choice of  $u_{0s}$  depends on the behavior of the solution at  $x \rightarrow -\infty$ . For the square root in (3.2) to be real at  $x = -\infty$ , we require that

$$(3.3) \quad u_{0s} = \zeta \left( 2 \sqrt{2 \int_{-\infty}^0 f(y, u_{0s}) dy} \right)$$

with some  $\zeta \geq 1$ . The effect of  $\zeta$ , which is the analogue of the overdrive factor in detonation theory, on the shape and the stability of the traveling wave can be readily appreciated in the nondimensional formulation given in section 4. The case with  $\zeta = 1$ , whereby

$$(3.4) \quad u_{0s} = 2\sqrt{2 \int_{-\infty}^0 f(y, u_{0s}) dy},$$

is an important special case commonly referred to as the CJ solution, because the characteristic speed at  $x = -\infty$  is  $c_0(-\infty) = u_0(-\infty) - u_{0s}/2 = 0$ . Therefore, the characteristics point toward the shock everywhere at  $x < 0$ , becoming vertical at  $x = -\infty$ . Cases where  $\zeta > 1$  are related to piston-driven detonations wherein the state at  $x = -\infty$  remains subsonic, i.e.,  $c > 0$ . In the context of the Euler detonations, they are known to be more stable than CJ waves [25, 37].

**3.2. Spectral stability of the steady-state solution.** Consider the linear stability of the steady-state solution obtained in the previous section. For simplicity, we limit the analysis to the CJ case, but the overdriven solution can be similarly analyzed. Let  $u(x, t) = u_0(x) + \epsilon u_1(x, t) + O(\epsilon^2)$  with  $\epsilon \rightarrow 0$ , and linearize (2.6). We find that

$$(3.5) \quad u_{1t} + \left(u_0 - \frac{u_{0s}}{2}\right) u_{1x} + u_0' u_1 = \left(\frac{\partial f}{\partial u_s}(x, u_{0s}) + \frac{u_0'}{2}\right) u_1(0, t).$$

The steady-state characteristic speed is

$$(3.6) \quad c_0 = u_0 - \frac{u_{0s}}{2} = \sqrt{2 \int_{-\infty}^x f(y, u_{0s}) dy},$$

and the coefficient on the right-hand side of the linearized equation above is

$$(3.7) \quad b_0 \equiv \frac{\partial f}{\partial u_s}(x, u_{0s}) + \frac{u_0'}{2} = \frac{\partial f}{\partial u_s}(x, u_{0s}) + \frac{f(x, u_{0s})}{2c_0(x)} = \frac{\partial f}{\partial u_s}(x, u_{0s}) + \frac{1}{2}c_0'(x).$$

Both  $c_0$  and  $b_0$  are functions of  $x$ .

Thus, the linear stability problem requires that the following linear nonlocal PDE with variable coefficients,

$$(3.8) \quad u_{1t} + c_0 u_{1x} + c_0' u_1 = b_0 u_1(0, t),$$

be solved subject to appropriate initial data,  $u_1(x, 0)$ . If spatially bounded (in some norm, to be defined below) solutions of (3.8) grow in time, then instability is obtained. At this point, we can proceed with either the Laplace transform in time (as in [7]) or normal modes (as in [25]). We choose the latter and substitute the normal modes,

$$(3.9) \quad u_1 = \exp(\sigma t) v(x),$$

into (3.8) to obtain

$$c_0 v' + c_0' v + \sigma v = b_0(x) v(0).$$

This equation can be integrated directly to yield

$$\exp\left(\sigma \int_0^x \frac{dy}{c_0(y)}\right) c_0(x) v(x) - c_0(0) v(0) = v(0) \int_0^x b_0(\xi) \exp\left(\sigma \int_0^\xi \frac{dy}{c_0(y)}\right) d\xi.$$

Denoting  $p = \int_x^0 dy/c_0(y) > 0$ , we obtain the final solution for the amplitude of the normal mode:

$$(3.10) \quad v(x) = v(0)p'(x)e^{\sigma p(x)} \left[ \int_x^0 b_0(\xi)e^{-\sigma p(\xi)} d\xi - c_0(0) \right].$$

The existence of an unstable eigenvalue with  $\Re(\sigma) > 0$  and bounded  $v(x)$  is equivalent to normal-mode instability. On physical grounds, we require that  $f$  be integrable in  $x$  at any given  $t$  (i.e., the  $L^1$  norm of  $f$  is bounded). This requirement follows from the implicit assumption that  $f$  is in fact the  $x$ -derivative of some reaction progress variable,  $\lambda$ , varying between 0 and 1. We impose the same constraint on  $u$ ; hence  $v \in L^1(\mathbb{R}^-)$ .

Note that  $p(x) \rightarrow \infty$  as  $x \rightarrow -\infty$ ; therefore, the factor in front of the brackets in (3.10) tends to infinity as  $x \rightarrow -\infty$ . To prevent this superexponential growth, the term in the brackets must vanish as  $x \rightarrow -\infty$ . In fact, this condition is also sufficient for instability.

**THEOREM 1.** *Provided that  $\|b_0(x)\|_{L^1} < \infty$ , the existence of a  $\sigma$  with  $\Re(\sigma) > 0$  such that*

$$(3.11) \quad \int_{-\infty}^0 b_0(\xi)e^{-\sigma p(\xi)} d\xi - c_0(0) = 0$$

*is both necessary and sufficient for the existence of unstable normal modes, (3.9).*

*Proof.* If condition (3.11) is not satisfied, then  $v(x) \rightarrow \infty$  as  $x \rightarrow -\infty$ . Now, suppose that (3.11) is satisfied. Then,  $v(x)$  takes the form

$$(3.12) \quad v(x) = \frac{v(0)}{c_0(x)} \int_{-\infty}^x b_0(\xi)e^{-\sigma(p(\xi)-p(x))} d\xi.$$

We now show that  $\|v(x)\|_{L^1} < \infty$ . From (3.12), it follows that

$$\begin{aligned} \|v\|_{L^1} &= |v(0)| \int_{-\infty}^0 dx \frac{1}{|c_0(x)|} \left| \int_{-\infty}^x b_0(\xi)e^{-\sigma(p(\xi)-p(x))} d\xi \right| \\ &\leq |v(0)| \int_{-\infty}^0 d\xi \int_{\xi}^0 dx \frac{1}{|c_0(x)|} |b_0(\xi)| e^{-\Re(\sigma)(p(\xi)-p(x))}. \end{aligned}$$

We change the integration variable in the inner integral from  $x$  to  $z = p(\xi) - p(x)$ , so that  $dx = -dz/p'(x) = c_0(x) dz$ . Then,

$$(3.13) \quad \|v\|_{L^1} \leq |v(0)| \int_{-\infty}^0 d\xi \int_0^{p(\xi)-p(0)} dz |b_0(\xi)| e^{-\Re(\sigma)z} \leq \frac{|v(0)|}{\Re(\sigma)} \|b_0\|_{L^1},$$

which proves that the unstable perturbations are bounded in the  $L^1$  norm, provided that  $b_0 \in L^1(\mathbb{R}^-)$ . Thus, (3.11) is necessary and sufficient for the existence of unstable normal modes.  $\square$

It is interesting that the dispersion relation (3.11) closely resembles that of [3, 4], where the detonation dynamics is analyzed in the asymptotic limit of strong overdrive. In this limit, the entire flow downstream of the lead shock has a small Mach number relative to the shock; hence the postshock pressure remains nearly constant. For this reason, such approximation is called quasi-isobaric. However, the underlying assumptions in the present model and those in the quasi-isobaric theory are quite

different. For example, in [3, 4], the authors assume that the detonation overdrive (i.e., the detonation speed normalized by the CJ speed) is large and that the ratio of specific heats is close to unity. The weak nonlinearity in [32], on the other hand, comes from the small heat release assumption there.

Another important result is that, under appropriate assumptions on  $f$ , the unstable modes have a bounded growth rate. This result shows that the so-called “pathological” instability, inherent to square-wave models of detonation in the Euler equations [43, 8, 11, 19], does not occur in our model for smooth steady-state solutions. However, in section 4.2.2 we show that this pathological instability occurs in the square-wave limit of our model, when  $f$  is replaced by a delta function.

**THEOREM 2.** *Provided that  $\|b_0 c_0\|_{L^\infty} = M < \infty$ , there exist no eigenvalues with  $\sigma_r > M/c_0(0)$ .*

*Proof.* Notice that

$$\left| \int_{-\infty}^0 b_0(x) e^{-\sigma p(x)} dx \right| \leq \int_{-\infty}^0 |b_0(x) e^{-\sigma p(x)}| dx = \int_{-\infty}^0 |b_0(x) e^{-\sigma_r p(x)}| dx.$$

Let  $z = p(x)$  and note that this function is invertible since  $p$  is monotonic. Substitution into the previous integral yields

$$\begin{aligned} \int_{-\infty}^0 |b_0(x) e^{-\sigma_r p(x)}| dx &= \int_0^\infty |b_0(p^{-1}(z)) c_0(p^{-1}(z))| e^{-\sigma_r z} dz \\ &\leq \max_{-\infty \leq x \leq 0} |b_0 c_0| \int_0^\infty e^{-\sigma_r z} dz = \frac{1}{\sigma_r} \max_{-\infty \leq x \leq 0} |b_0 c_0|, \end{aligned}$$

and thus for  $\sigma_r > (\max_{-\infty \leq x \leq 0} |b_0 c_0|) / c_0(0)$ , we obtain

$$\left| \int_{-\infty}^0 b_0(x) e^{-\sigma p(x)} dx \right| \leq \frac{1}{\sigma_r} \max_{-\infty \leq x \leq 0} |b_0 c_0| < c_0(0).$$

This contradicts the dispersion relation stated in Theorem 1.  $\square$

If  $f(x, u_{0s})$  is integrable and bounded and  $\frac{\partial f}{\partial u_s}(x, u_{0s})$  is bounded, then it can be shown that  $b_0 c_0 \in L^\infty$ . These constraints are sufficient to eliminate the pathological instabilities in which arbitrarily large growth rates are present.

**THEOREM 3.** *If  $\|b_0 c_0\|_{L^\infty} = M < \infty$ , there exists a bounded interval  $I$  large enough that all eigenvalues with  $\sigma_r > 0$  have imaginary part  $|\sigma_i| < I$ .*

*Proof.* By application of the Riemann–Lebesgue lemma, we find that

$$\begin{aligned} \int_{-\infty}^0 b_0(x) e^{-\sigma p(x)} dx &= \int_0^\infty b_0(x) c_0(x) e^{-\sigma z} dz \\ &= \int_0^\infty (b_0(x) c_0(x) e^{-\sigma_r z}) e^{i\sigma_i z} dz \rightarrow 0 \quad \text{as } \sigma_i \rightarrow \infty, \end{aligned}$$

provided that  $b_0(p^{-1}(z)) c_0(p^{-1}(z)) e^{-\sigma_r z} \in L^1$ . If  $\sigma_r > 0$  and  $b_0 c_0$  is bounded, then it follows that indeed  $b_0(p^{-1}(z)) c_0(p^{-1}(z)) e^{-\sigma_r z} \in L^1$ . Therefore, the integral above vanishes as  $\sigma_i \rightarrow \infty$ , which cannot happen because the integral should be equal to  $c_0(0) = u_{0s}/2 > 0$ .  $\square$

**THEOREM 4.**  $\sigma = 0$  is never an eigenvalue.

*Proof.* The condition  $\int_{-\infty}^0 b_0(\xi) e^{-\sigma p(\xi)} d\xi - c_0(0) = 0$  is still necessary for the eigenfunctions to remain bounded, even when  $\sigma = 0$ . Therefore,  $\int_{-\infty}^0 b_0(\xi) d\xi -$



$c_0(0) = 0$ , or equivalently

$$\int_{-\infty}^0 \left[ \frac{\partial f}{\partial u_s}(\xi, u_{0s}) + \frac{1}{2} c_0(\xi)' \right] d\xi - c_0(0) = 0,$$

$$\int_{-\infty}^0 \frac{\partial f}{\partial u_s}(\xi, u_{0s}) d\xi = \frac{c_0(0)}{2}.$$

Since we assume that  $f$  integrates to a constant, then

$$\int_{-\infty}^0 \frac{\partial f}{\partial u_s}(\xi, u_{0s}) d\xi = \frac{d}{du_s} \int_{-\infty}^0 f(\xi, u_{0s}) d\xi = 0.$$

But  $c_0(0) = u_{0s}/2 > 0$ , and therefore no such eigenvalue can exist. Thus, at the onset of instability, the eigenvalues must have nonzero frequency.  $\square$

Because  $\sigma = 0$  is never an eigenvalue, when the behavior of the system as a function of parameters is explored, the transition from a stable steady state to instability usually involves a Hopf bifurcation. In our numerical calculations we find that this bifurcation is a supercritical Hopf bifurcation, so that a stable time periodic solution takes over from the steady state.

**4. An example.** In the previous section, we presented necessary and sufficient conditions for the normal-mode instability of a traveling wave profile. We now focus on a specific choice of  $f(x, u_s)$  and illustrate with it the general results on the linear instability. We also examine, by means of direct numerical simulations, what happens once the traveling-wave solution becomes unstable as a bifurcation parameter is varied. The example mimics, on a qualitative level, a situation wherein the chemical reaction has an induction zone that delays the beginning of an energetic exothermic reaction. The idea is to have a function that peaks at some distance away from the shock, with this distance depending on the shock strength. A simple choice for such a function is

$$(4.1) \quad f = \frac{q}{2} \frac{1}{\sqrt{4\pi\beta}} \exp \left[ -\frac{(x - x_i(u_s))^2}{4\beta} \right].$$

Here,  $x_i$  is the point where  $f$  peaks, and that point depends on the current state at the shock,  $u_s = u(0, t)$ . The parameter  $\beta$  determines the width of the reaction zone. As  $\beta \rightarrow 0$ ,  $f$  tends to  $\frac{q}{2} \delta(x - x_i)$ ; this limit yields what is called a square-wave profile, wherein  $f$  kicks in only at  $x = x_i$ . We choose  $x_i$  as

$$(4.2) \quad x_i(t) = -k \left( \frac{u_{0s}}{u_s(t)} \right)^\alpha,$$

which depends on the shock strength,  $u_s$ ; the steady-state shock strength,  $u_{0s}$ ; and the parameters  $k > 0$  and  $\alpha \geq 0$ . Remembering the connection with the weakly nonlinear model, where  $f = q\lambda_x/2$ , we require that

$$(4.3) \quad \int_{-\infty}^0 f(x, u_s) dx = \frac{q}{2},$$

and thus renormalize  $f$  as follows:<sup>1</sup>

$$f \rightarrow \frac{q}{2} \frac{f}{\int_{-\infty}^0 f dx} = \frac{q}{\left( 1 + \operatorname{Erf} \left[ k \left( \frac{u_s}{u_{0s}} \right)^{-\alpha} / 2\sqrt{\beta} \right] \right) \sqrt{4\pi\beta}} \exp \left[ -\frac{(x + k(u_{0s}/u_s)^\alpha)^2}{4\beta} \right].$$

<sup>1</sup>Note that in [22, 23],  $f$  was not renormalized.

Next, the variables are rescaled as follows:  $u = u_{0s}\tilde{u}$ ,  $x = k\tilde{x}$ ,  $t = k\tilde{t}/u_{0s}$ , and  $\beta = k^2\tilde{\beta}$ , where the variables with the tildes are now dimensionless. Using  $u_{0s} = 2\zeta\sqrt{q}$ , which follows from (3.3) and (4.3), equation (2.6) takes the dimensionless form

$$(4.4) \quad \tilde{u}_{\tilde{t}} + \left( \frac{\tilde{u}^2}{2} - \frac{\tilde{u}\tilde{u}(0, \tilde{t})}{2} \right)_{\tilde{x}} = \tilde{f}(\tilde{x}, \tilde{u}_s),$$

where

$$(4.5) \quad \tilde{f}(\tilde{x}, \tilde{u}_s) = \frac{1}{4\zeta^2 \left( 1 + \text{Erf} \left[ \tilde{u}(0, \tilde{t})^{-\alpha} / 2\sqrt{\tilde{\beta}} \right] \right)} \frac{1}{\sqrt{4\pi\tilde{\beta}}} \exp \left[ -\frac{(\tilde{x} + (\tilde{u}(0, \tilde{t}))^{-\alpha})^2}{4\tilde{\beta}} \right].$$

This equation contains only three parameters:  $\alpha$ , which is a measure of the shock-state sensitivity of the source function (analogous to the activation energy in Euler detonations);  $\tilde{\beta} = \beta/k^2$ , which is the width of  $f$  (analogous to the ratio of the reaction-zone length,  $\sqrt{\beta}$ , and the induction-zone length,  $k$ ); and  $\zeta$ , which is the overdrive factor. The role of  $\zeta$  is now easily appreciated: it scales the forcing term by  $\zeta^{-2}$  such that the overdrive reduces the magnitude of the forcing and hence has a stabilizing effect.

Our focus below is on the CJ case,  $\zeta = 1$ , which leaves only  $\alpha$  and  $\beta$  as the parameters of the model. Although the expression for the forcing is a little bit cumbersome, its shape is simply that of a Gaussian shifted to the left of  $x = 0$  by  $\tilde{u}(0, \tilde{t})^{-\alpha}$  and renormalized to integrate to a constant on  $(-\infty, 0)$ . A few examples of  $f$  are shown in Figure 4.1(a) for different values of  $u_s$  and fixed  $\alpha, \beta$ . The main qualitative feature of  $f$  is that it has a maximum at some distance from  $x = 0$  and that the maximum is close to the shock when  $u_s$  is large and far from the shock when  $u_s$  is small. These features mimic the behavior of the reaction rate in the Euler equations as a function of the lead-shock speed.

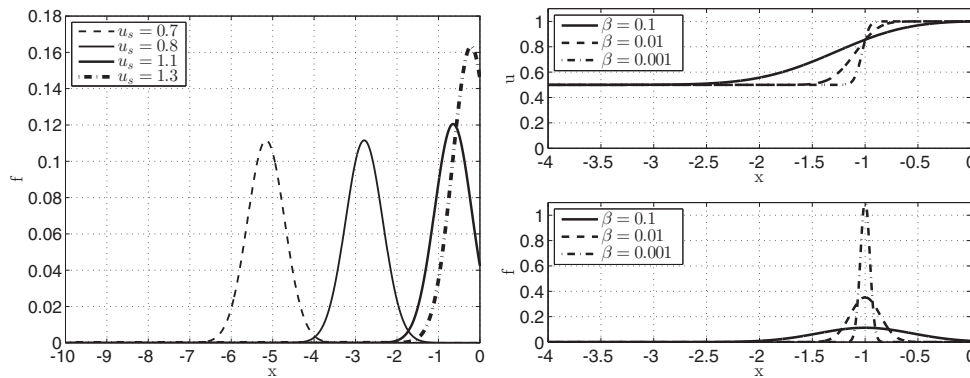


FIG. 4.1. (a) The forcing term at various  $u_s$ . (b) The steady-state profiles (top) and the forcing function (bottom) as  $\beta$  is varied.

From now on, we drop the tilde notation, but it should be understood that all the variables below are dimensionless.

**4.1. Steady-state solutions.** Steady-state CJ solutions can be computed as shown in section 3.1. Figure 4.1(b) shows how  $\beta$  affects the traveling wave profile.

The picture suggests a square-wave solution in the limit  $\beta \rightarrow 0$ . It is important to remember that  $\alpha$  plays no role in the steady-state profiles because  $u_{0s} = 1$  in dimensionless form. In some sense,  $\alpha$  represents the sensitivity to changes in the steady-state profile. Next, we study the linear stability of these traveling wave profiles in the  $\alpha - \beta$  parameter space.

## 4.2. Linear stability analysis.

**4.2.1. The dispersion relation.** By Theorem 1, spectral instability is equivalent to (3.11), provided  $\|b_0\|_{L^1} < \infty$ . A straightforward computation shows that

$$\|b_0\|_{L^1} = \int_{-\infty}^0 \left| \frac{\partial f}{\partial u_s}(x, u_{0s}) + \frac{f(x, u_{0s})}{2c_0(x)} \right| dx < \infty,$$

and therefore spectral stability of (4.4) is equivalent to

$$\int_{-\infty}^0 b_0(\xi) e^{-\sigma p(\xi)} d\xi = c_0(0),$$

where  $b_0$ ,  $c_0$ , and  $p$  are defined as in section 3.2. Although we have reduced the spectral stability of our problem to finding complex roots of a single equation, the equation is (although analytic in  $\sigma$ ) numerically difficult. For a given  $\alpha$  and  $\beta$ , an equation with three levels of nested integration must be solved,

$$(4.6) \quad \int_{-\infty}^0 \left\{ \left( \frac{\partial f(\xi, u_{0s})}{\partial u_s} + \frac{\partial}{\partial \xi} \sqrt{\frac{1}{2} \int_{-\infty}^{\xi} f(y, u_{0s}) dy} \right) \exp \left[ -\sigma \int_{\xi}^0 \frac{dx}{\sqrt{2 \int_{-\infty}^x f(y, u_{0s}) dy}} \right] \right\} d\xi = \frac{u_{0s}}{2},$$

where  $\sigma = \sigma_r + i\sigma_i$  and  $f$  is given by (4.5). Interestingly, the original formulation of the linear stability problem by Erpenbeck [7] requires the same three levels of numerical integration (the steady-state solution, then the solution of the adjoint homogeneous problem, and then the evaluation of the dispersion relation). In general, these integrals require nearly machine-precision evaluation of the functions in the integrands in order to obtain the eigenvalues with only a few significant digits of accuracy. Except for the limiting case of  $\beta = 0$ , we find the roots numerically using the *fsolve* function of MATLAB, which uses a version of Newton's method, and then we use Cauchy's argument principle to verify that we have found all the roots in a given region of the complex plane. Here, Theorem 2 plays a fundamental role, since it tells us that all eigenvalues must be within a finite region. When  $\beta = 0$ , we compute the roots analytically, and they serve as initial guesses in the numerical continuation root-finding procedure when  $\beta$  is small.

**4.2.2. The square-wave limit.** When  $\beta \rightarrow 0$ , we obtain the square-wave solution. In this limit, it can be shown that

$$\frac{\partial}{\partial u_s} f(x, u_{0s}) = -\alpha \frac{\partial}{\partial x} f(x, u_{0s}) + O\left(\frac{1}{\sqrt{\beta}} e^{-\frac{1}{4\beta}}\right) f(x, u_{0s}).$$

Even though  $f(x, u_{0s})$  tends to a delta function when  $\beta \rightarrow 0$ , this function is integrated in the dispersion relation, and therefore the contribution of the second

term above to the dispersion relation is exponentially small in the limit due to the  $O(\frac{1}{\sqrt{\beta}}e^{-\frac{1}{4\beta}})$  factor. In the limit, the dispersion relation (3.11) becomes

$$\begin{aligned} \int_{-\infty}^0 b_0(x) e^{-\sigma p(x)} dx &= \int_{-\infty}^0 \left( \frac{\partial f}{\partial u_s}(x, u_{0s}) + \frac{1}{2} \frac{\partial}{\partial x}(c_0(x)) \right) e^{-\sigma p(x)} dx \\ &= \int_{-\infty}^0 \left( -\alpha \frac{\partial f}{\partial x}(x, u_{0s}) \right) e^{-\sigma p(x)} dx \\ &\quad + \int_{-\infty}^0 \left( \frac{1}{2} \frac{\partial}{\partial x}(c_0(x)) \right) e^{-\sigma p(x)} dx. \end{aligned}$$

Integrating by parts and performing simple algebraic manipulations, we find that

$$\begin{aligned} -\alpha \int_{-\infty}^0 \frac{\partial f}{\partial x}(x, u_{0s}) e^{-\sigma p(x)} dx + \frac{1}{2} \int_{-\infty}^0 \frac{\partial}{\partial x}(c_0(x)) e^{-\sigma p(x)} dx &= c_0(0), \\ -\alpha f(0, u_{0s}) + \alpha \sigma c_0(0) - \left( \alpha \sigma^2 + \frac{\sigma}{2} \right) \int_0^\infty c_0(x) e^{-\sigma z} dz &= \frac{c_0(0)}{2}. \end{aligned}$$

Noticing that

$$c_0(x) \rightarrow \begin{cases} \frac{1}{2}, & x \geq -1, \\ 0, & x < -1, \end{cases}$$

and

$$p(x) = \int_x^0 \frac{dy}{c_0(y)} \rightarrow \begin{cases} \infty, & x < -1, \\ -2x, & x \geq -1, \end{cases}$$

we obtain

$$\begin{aligned} \lim_{\beta \rightarrow 0} \left[ -\alpha f(0, u_{0s}) + \alpha \sigma c_0(0) - \left( \alpha \sigma^2 + \frac{\sigma}{2} \right) \int_0^\infty c_0(p^{-1}(z)) e^{-\sigma z} dz - \frac{c_0(0)}{2} + o(1) \right] \\ = \frac{\alpha \sigma}{2} - \left( \frac{\alpha \sigma^2}{2} + \frac{\sigma}{4} \right) \int_0^2 e^{-\sigma x} dx - \frac{1}{4} \\ = \left( \frac{\alpha \sigma}{2} + \frac{1}{4} \right) e^{-2\sigma} - \frac{1}{2} \\ = 0. \end{aligned}$$

Therefore, the dispersion relation in the square-wave limit takes a very simple form of a transcendental equation,

$$(4.7) \quad e^{2\sigma} = \alpha \sigma + \frac{1}{2}.$$

This dispersion relation has exactly the same form as that of Fickett’s analogue [11], which in his case arose from his differential-difference equation for shock perturbation. Therefore, it predicts the same pathological instability as in the classical square-wave detonations. Pathological instability implies that the linear stability problem for the square wave is ill-posed in the sense of Hadamard. For completeness, we exhibit below the solutions to this equation, since they are used as initial guesses in our algorithm

to compute the solutions when  $\beta$  is small but not zero. Let  $\sigma = \sigma_r + i\sigma_i$ , and separate the real and imaginary parts of (4.7):

$$e^{2\sigma_r} \cos(2\sigma_i) = \alpha\sigma_r + \frac{1}{2}, \quad e^{2\sigma_r} \sin(2\sigma_i) = \alpha\sigma_i.$$

If  $\sigma_r$  is to be large, the first equation requires  $\cos(2\sigma_i)$  to be small; i.e.,  $\sigma_i$  should be close to  $\pi/4 + n\pi/2$ ,  $n = 0, 1, 2, \dots$ . We let

$$(4.8) \quad \sigma_i = \frac{\pi}{4} + \frac{n\pi}{2} + \varepsilon,$$

where  $\varepsilon$  is a small correction. Then, from the second equation, we find  $\sin(2\sigma_i) \approx 1$  and therefore  $\sigma_r \approx \frac{1}{2} \ln(\alpha\sigma_i)$ . For this  $\sigma_r$  to be large, we need  $n$  to be large, in which case

$$(4.9) \quad \sigma_r \approx \frac{1}{2} \ln(n).$$

Thus, the square-wave dispersion relation admits arbitrarily large growth rates that occur at simultaneously large frequencies. It is interesting that the growth rate increases with frequency logarithmically. Similar growth happens in the square-wave model of detonations in the reactive Euler equations (see, e.g., [43, 8, 2, 34, 35, 19]). However, in the latter, the dispersion relation involves several exponential functions due to the presence of multiple time scales associated with different families of waves propagating from the shock into the reaction zone. Waves of different families of characteristics propagate at different speeds, resulting in several different time intervals for the signals to propagate from the shock to the “fire” and back. Since in the limit of large frequencies one of the exponentials dominates, the dispersion relation becomes essentially the same as in our model. In the numerical calculations of detonation instability in the Euler equations with finite-rate chemistry but high activation energies [35], a similarly slow growth can be seen. However, we do not know whether the growth is logarithmic in frequency.

*Remark.* Theorem 2 is not contradicted here since  $\|b_0c_0\| \notin L^\infty$  in the limit, because now  $f \notin L^\infty$ .

**4.2.3. The unstable spectrum for  $\beta > 0$ .** The pathological instability of the model as  $\beta \rightarrow 0$  was shown to be caused by an infinite number of unstable eigenvalues, with the real part arbitrarily large. From Theorem 2, we know that if  $\|b_0c_0\|_{L^\infty} = M < \infty$ , then there can be no unstable eigenvalues with  $\sigma_r > M/c_0(0)$ . A quick computation shows that if  $\alpha < \infty$  and  $\beta > 0$ , then the real part of the unstable spectrum of (4.4) is bounded from above.

Next, we fix  $\alpha = 4.05$  and numerically investigate the effect of  $\beta$  on the eigenvalues. Using as an initial guess the eigenvalues found from the square-wave dispersion relation, (4.7), we use the numerical root finder, *fsolve*, from MATLAB to locate the eigenvalues for successively larger values of  $\beta$ . Figure 4.2(a) shows the results, reaffirming that for any value of  $\beta > 0$  there are only a finite number of unstable eigenvalues. Furthermore, it suggests that the magnitude of  $\beta$  is closely related to the frequencies of the unstable eigenvalues. This can be understood as follows: as the shock is perturbed, it creates waves that propagate into the reaction zone. If  $\beta$  is large enough, the reaction zone is smooth, and there is little resonance between the shock and the peak of the reaction in the reaction zone. However, as  $\beta$  is decreased, the sharp peak in the reaction zone reflects waves back to the shock, and this resonance

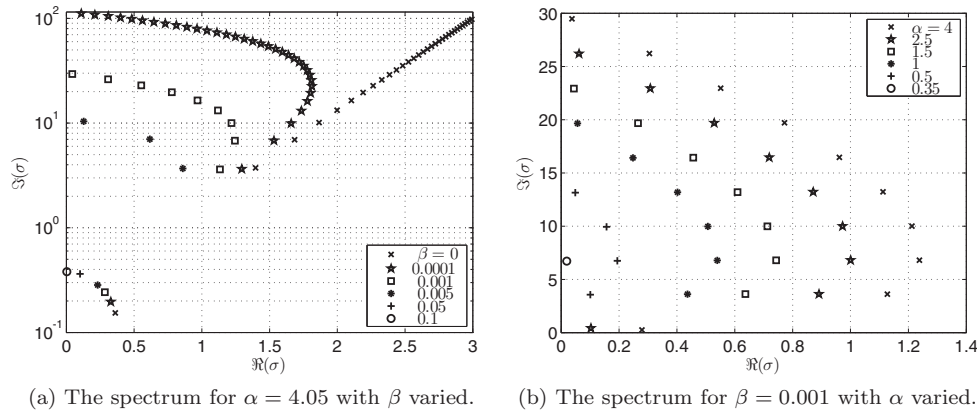


FIG. 4.2. The linear spectrum.

causes the instability. If  $\beta$  is small but positive, then high enough frequencies do not “see” the sharp peak in the reaction rate and are not reflected back to the shock. A similar mechanism is at work in Euler detonations as well. For example, in [36], as the length of the main heat-release layer is decreased relative to that of the induction zone, the detonation is found to become more unstable.

We also look at the effect of  $\alpha$  on the distribution of the eigenvalues. In Figure 4.2(b), we show the spectrum for fixed  $\beta = 0.001$  and varying  $\alpha$ . This figure suggests that the eigenvalues are merely shifted when  $\alpha$  is decreased. Interestingly, the imaginary part of the dominant eigenvalue, i.e., the one with the largest real part, is always the same as we change  $\alpha$  and keep  $\beta$  fixed. This observation was tested for different values of  $\beta$ . As  $\beta$  decreases, the frequency of the most unstable mode is seen to increase.

To ensure that no roots of the dispersion relation have been lost in the numerical computations, we apply the argument principle to (3.11). Since

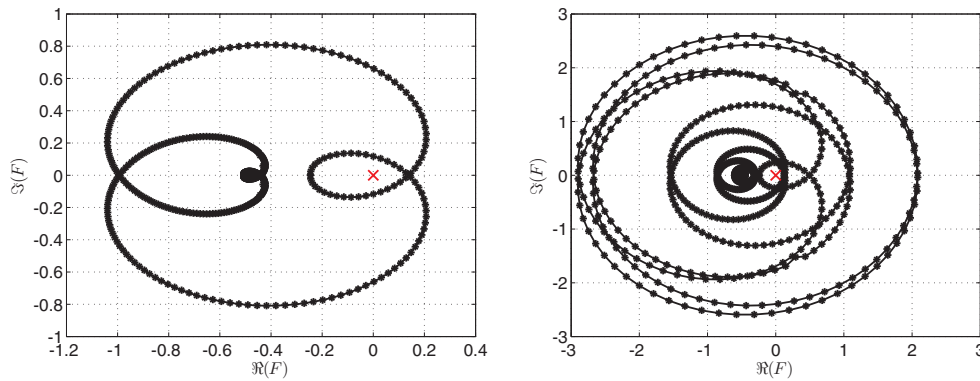
$$F(\sigma) = \int_{-\infty}^0 b_0(\xi) e^{-\sigma p(\xi)} d\xi - c_0(0)$$

has no poles in the region  $\sigma_r \geq 0$  (which follows from  $\|b_0\|_{L_1} < \infty$ ), the argument principle guarantees that the number of zeroes,  $N$ , of  $F(\sigma)$  in a closed contour  $C$  (counting multiplicity) is given by

$$(4.10) \quad N = \frac{1}{2\pi i} \int_C \frac{F'(z)}{F(z)} dz.$$

This can be related to the winding number of a curve by the substitution  $w = F(z)$ , which yields  $N = \frac{1}{2\pi i} \int_{F(C)} dw/w$ . We show in Figure 4.3 two Nyquist plots of the dispersion relation, corresponding to parameters with 2 and 20 unstable eigenvalues. The predictions agree with the number of roots found using the root solver.

**4.2.4. The neutral curves.** We follow the first five unstable eigenvalues (ordered according to their imaginary part) and show their neutral curves in Figure 4.4. We see that for large values of  $\beta$  the lowest frequency eigenvalue is the one that first becomes unstable, but for very small values of  $\beta$  the stability of the traveling wave is controlled by the higher frequency perturbations. Moreover, the smaller the  $\beta$ , the



(a)  $\alpha = 4.05, \beta = 0.05$ . Weakly unstable case with two eigenvalues, one shown in Figure 4.2 and the other its complex conjugate.

(b)  $\alpha = 4.05, \beta = 0.005$ . Highly unstable case with twenty eigenvalues, ten shown in Figure 4.2 and their complex conjugates.

FIG. 4.3. Values of  $w = F(z)$  along a large semicircle in the right-half plane of the  $z$ -plane (radius 10 for 4.3(a) and 100 for 4.3(b)), plotted in the  $F$ -plane. The total number of loops around the origin in the  $F$ -plane gives the winding number, which is equal to the number of unstable eigenvalues.

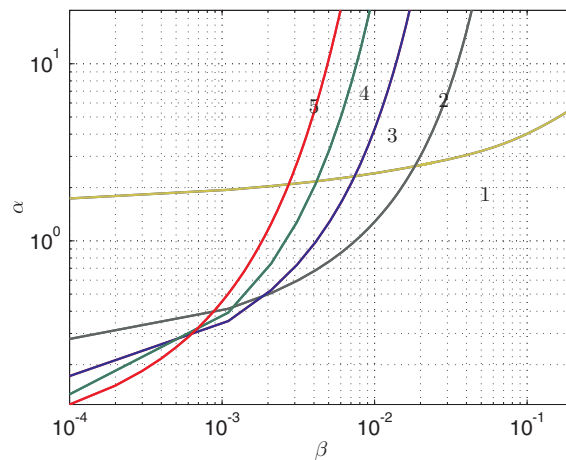


FIG. 4.4. The neutral curves for the first five eigenvalues. The numbers next to each curve correspond to the index of the eigenvalue. Below the envelope of the curves, we have discrete spectral stability; in fact, numerical calculations indicate that the solutions are stable at these parameters.

higher the frequency of the most unstable mode, consistent with our earlier calculation of the square-wave-limit pathology. The whole unstable region is given by the union of the unstable regions for each eigenvalue and is generally located at large-enough  $\alpha$  for any given  $\beta$ , or small-enough  $\beta$  for any given  $\alpha$ .

**4.3. Numerical simulations.** The previous section was concerned with the linear stability of traveling wave solutions of (4.4). We were able to compute the spectrum of unstable modes and obtain the neutral curves in the  $\alpha$ - $\beta$  parameter space. In this section, we investigate the behavior of solutions in the nonlinear regime by numerically solving the PDE using the WENO algorithm described in the appendix. All the simulations start with a steady-state solution, and instabilities (when present) are triggered by the numerical discretization error alone. The goal of this section

is to demonstrate that, as in detonation waves in the reactive Euler equations, the shock dynamics goes through a Hopf bifurcation followed by a period-doubling cascade when the sensitivity parameter,  $\alpha$ , is varied, suggesting a possible chaotic regime for large-enough  $\alpha$ .

**4.3.1. Linear growth and comparison with stability analysis.** We first compare the results obtained from the linear stability analysis with the numerical results from the simulation. We perform a least-squares fit on the deviation from the steady-state value of the form  $\sum_{k=1}^n c_k e^{\sigma_{r_k} t} \cos(\sigma_{i_k} t + \delta_k)$ , where  $n$  is the number of unstable eigenvalues found in the linear stability analysis. For instance, when  $\beta = 0.1$  and  $\alpha = 4.05$ , from Figure 4.2 we expect one unstable mode to appear, and thus, at least for a small time interval, we expect the solution to behave like  $e^{\sigma_k t}$ , up to translation and scaling. The results obtained from the comparison are presented in Table 4.1. We restrict ourselves to fitting up to two eigenvalues (eight parameters) and fit up to a time when the perturbation is of the order  $10^{-7}$ . The original perturbation is of the order  $10^{-15}$ .

TABLE 4.1

Comparison of eigenvalues from stability analysis and from numerics at  $\alpha = 4.05$ .

$\beta$	$\sigma$ from theory	$\sigma$ from numerics
0.10	$0.00309 + 0.38144i$	$0.00311 + 0.38152i$
0.01	$0.20092 + 0.30431i$	$0.20581 + 0.29964i$
	$0.61295 + 3.78512i$	$0.61298 + 3.78507i$

The first case of  $\beta = 0.1$  in Table 4.1 is near the neutral curve, and both the growth and frequency of the perturbation are well captured by the linear stability predictions. Simulations show that for this “slightly unstable” regime, the predicted frequency is valid well into the nonlinear regime, an observation often made in detonation simulations as well. In the second case, when  $\beta = 0.01$ , we see a larger discrepancy between the linear theory and the numerical simulations, especially when capturing the effect of the least unstable mode. This is to be expected, since the effects of all unstable modes except for the most unstable one quickly become negligible as the dominant mode starts to grow. This second case is far from the neutral curve and much more unstable, with a growth rate two orders of magnitude larger than in the first case. Very fast growth of the perturbations is likely to result in nonlinear effects starting to play an important role.

**4.3.2. Limit cycles and period-doubling bifurcations.** We now study the long-time asymptotic behavior of solutions that start from a small perturbation (given by the discretization error) of the initial steady-state solution. The shock value of the solution,  $u_s(t)$ , is analyzed. For all the simulations that follow, we fix  $\beta = 0.1$  and vary  $\alpha$ . When  $\alpha$  slightly exceeds the critical value  $\alpha_c \approx 4.02$ , predicted by the linear analysis as the neutral boundary, the numerical solutions show that the steady-state solution is unstable, with the long-time evolution leading to a limit cycle.

For a range of  $\alpha$  between  $\alpha_c$  and  $\alpha_1 \approx 4.72$ , the long-time dynamics is that of a simple limit cycle (Figure 4.5(a)). Subsequent increase of  $\alpha$  leads to a period-doubling bifurcation. When  $\alpha$  is between  $\alpha_1$  and  $\alpha_2 \approx 4.91$ , we observe the limit cycle shown in Figure 4.5(b). This period-doubling process continues until eventually, at  $\alpha = \alpha_\infty \approx 4.97$ , the solution (apparently) becomes chaotic. Figure 4.5(c) illustrates the behavior of  $u_s(t)$  for very large values of  $t$  (around 20,000), when all the transients are likely to have vanished. The respective power spectra, computed using a large



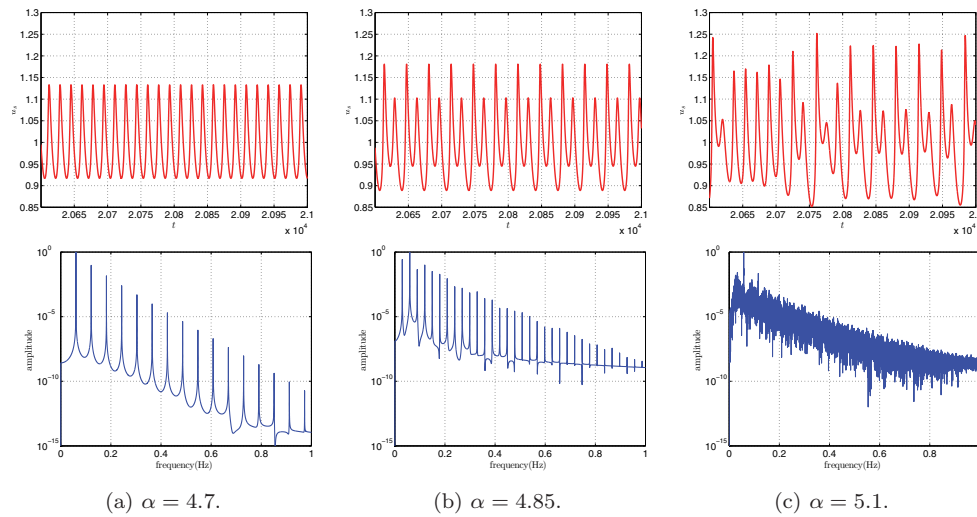


FIG. 4.5. Top row:  $u_s(t)$  for  $\beta = 0.1$  and different values of  $\alpha$ . Bottom row: corresponding power spectra.

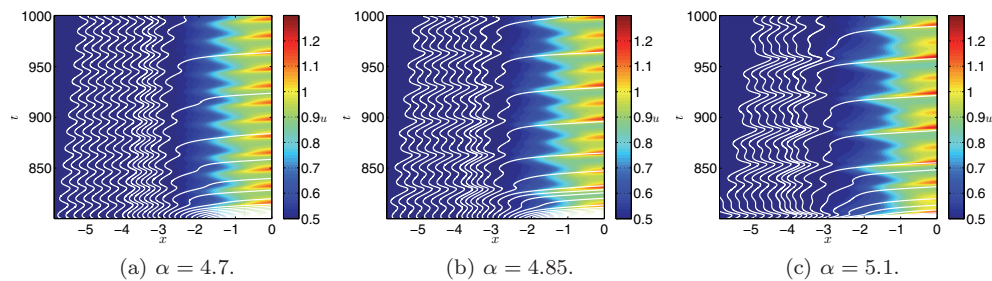
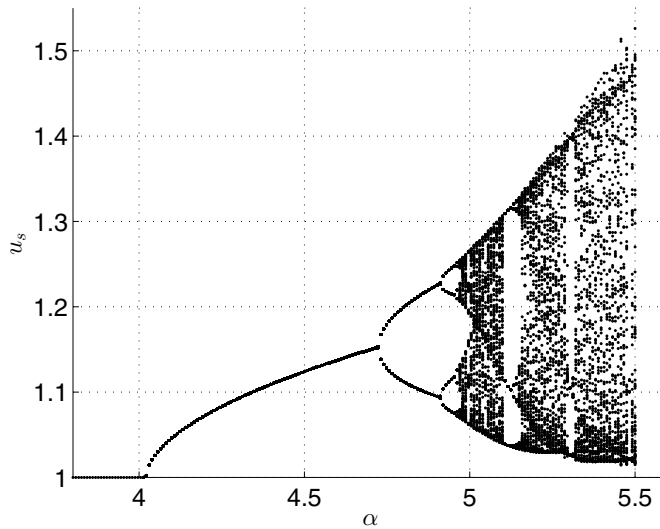


FIG. 4.6. Characteristic fields (white curves) at various  $\alpha$ , at periods 1, 2, and chaotic. The color shows the magnitude of  $u$ .

time window,  $10,000 < t < 22,000$ , are also shown. In the periodic case, the power spectrum is clearly marked by peaks in the natural frequency and its harmonics, as seen in Figure 4.5(a), (b). In Figure 4.5(c), although there is a dominant frequency in the signal, many other frequencies are present, indicating possible aperiodicity or chaos. Further analysis of the computational results is required to establish whether the solution is indeed chaotic, analysis which is done in the subsequent sections.

Although we focus on  $u_s(t)$ , the behavior presented in Figure 4.5 is not unique to the shock value. That said, we must pick an “interesting” point, meaning a point close enough to the shock, if we want to capture the rich dynamics. After the Hopf bifurcation occurs,  $u(x, t)$  is periodic in time, and as the bifurcation parameter ( $\alpha$  in this case) is increased further,  $u(x, t)$  appears to become chaotic. This is illustrated in Figure 4.6, where the color represents  $u(x, t)$  and the white lines are the characteristics.

The bifurcation process is best illustrated by means of a bifurcation diagram, where the local maxima of the shock value,  $u_s(t)$ , are plotted at different values of the bifurcation parameter  $\alpha$  (Figure 4.7). The bifurcation points, presented in Table 4.2,

FIG. 4.7. *The bifurcation diagram at  $\beta = 0.1$ .*TABLE 4.2  
*Bifurcation points.*

$n$	1	2	3	4	5
$\alpha_n$	4.02	4.7202	4.9100	4.95565	4.96553
$F_n$	...	...	3.69	4.16	4.62

are used to compute the Feigenbaum number, which appears to approach the well-known constant  $\delta \approx 4.669$ . The bifurcation diagram in Figure 4.7 and the power spectra in Figure 4.5 all suggest (although they do not prove) that the chaos in the system is real. In section 4.4, we analyze the apparently chaotic series of  $u_s(t)$  at very large  $t$ , i.e., on the attractor.

An interesting feature of the example presented above is that, as in the reactive Euler equations (e.g., [24]), inner shocks can form inside the smooth region,  $x < 0$ . These shocks subsequently overtake the leading shock, rendering its dynamics nonsmooth. The inner-shock formation is simply due to the wave breaking, and it depends on the initial data as well as the parameters in  $f$ . For example, as the parameter  $\alpha$ , which controls the shock-state sensitivity, is increased, the characteristics are seen to converge toward each other at large  $t$  until, at a critical value of  $\alpha$ , the characteristics collide into an inner shock. This shock then overtakes the leading shock at  $x = 0$ , as shown in Figure 4.8. A point to emphasize is that the characterization of chaos when such nonsmooth dynamics is present is not easy, particularly due to difficulties of computing the solution with high accuracy. Our analysis of chaos is therefore limited to moderate values of  $\alpha$ , when we know that the internal shock does not form yet a chaotic signal is observed.

**4.4. Time series analysis.** In this section, we use tools of dynamical systems to understand the shock signal. The shock signal represents a one-dimensional measurement of the infinite-dimensional phase space where the solutions live. Relying on

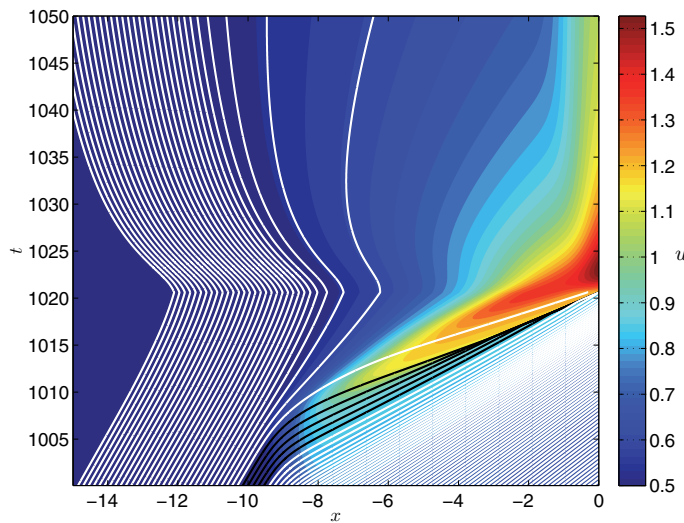


FIG. 4.8. Formation of an internal shock wave. The color shows the magnitude of  $u$ . The white curves are the forward characteristics.

Takens' theorem [39], we embed the signal in higher dimensions by choosing a delay,  $\tau$ , and an embedding dimension,  $m$  (note that choosing an appropriate  $\tau$  is a delicate question). We then use this embedded  $m$ -dimensional signal to compute quantities of interest, such as the correlation dimension and the largest Lyapunov exponent. The numerical calculations are performed using the open source software OPENTSTOOL [28].

**4.4.1. Delay reconstruction of the attractor.** We embed the signal  $u_s^n = u_s(t_n)$  in  $m$  dimensions by creating the points

$$\begin{aligned} p_1 &= (u_s^1, u_s^{1+\tau}, \dots, u_s^{1+(m-1)\tau}), \\ p_2 &= (u_s^2, u_s^{2+\tau}, \dots, u_s^{2+(m-1)\tau}), \\ &\vdots \\ p_N &= (u_s^N, u_s^{N+\tau}, \dots, u_s^{N+(m-1)\tau}), \end{aligned}$$

where  $N$  is limited by the number of available values of  $u_s$ . The  $m$ -dimensional points  $(p_1, \dots, p_N)$  then live in an attractor of dimension at most  $m$ . It was shown by Takens that, provided  $m > 2d + 1$ , where  $d$  is the dimension of the attractor where  $u_s$  lives, there exists a diffeomorphism between the reconstructed attractor and the "actual" attractor (in the limit of the infinite amount of noise-free data). This immediately allows us to use the reconstructed attractor to compute quantities such as the correlation dimension and the Lyapunov spectrum.

Notice that although in theory any choice of  $\tau$  will allow such reconstruction, in practice the situation is quite delicate. The finite amount of noise-polluted data makes the choice of  $\tau$  a nontrivial issue, still the subject of much current research. Since no fail-proof method appears to exist, we choose  $\tau$  as the first minimum of the mutual information function of  $u_s$ . The reasons for such a choice can be found in [16]. In the next subsection, we explore how the reconstructed attractor, its dimension, and

the largest Lyapunov exponent (LLE) change as we vary the sensitivity parameter,  $\alpha$ . We choose  $\alpha = 4.7, 4.85, 4.96, 4.97, 5, 5.1$  and see how these quantities change as the dynamics goes from periodic to chaotic.

**4.4.2. Largest Lyapunov exponent (LLE).** A chaotic system is characterized by at least one positive Lyapunov exponent. This means that information must be lost in the system as time progresses. Predictability is thus highly limited. Because the largest Lyapunov exponent (LLE) determines the dominant rate at which information is lost, we are primarily interested in the LLE. The magnitude of the LLE gives an indication of how quickly nearby trajectories in the phase space diverge as time progresses. The inverse of the LLE is an estimate of the relevant time scale for this divergence. Thus, the larger the LLE, the more chaotic the dynamics. In particular, Table 4.3 shows how sensitive this exponent is to small changes in the parameter  $\alpha$  near the onset of chaos, where  $\alpha$  is the “activation energy” parameter, measuring the sensitivity of the reaction to the shock strength. Several methods are available for computing the LLE, and we choose to use the one presented in [33]. The algorithm used here is discussed in the appendix.

The sequence of period doubling observed in Figure 4.7 and Table 4.2 suggests that the sequence first saturates at  $\alpha_c \approx 4.97$ . After this critical value, the solution seems to become aperiodic, as indicated by its power spectrum. We compute the LLE for values of  $\alpha$  slightly below and slightly above  $\alpha_c$  in order to illustrate the drastic change in the magnitude of LLE. The values of LLE are presented in Table 4.3, where the error estimates are merely educated guesses of a confidence interval obtained from running the algorithm for different embedding dimensions (from dimension 3 to 10). It is particularly difficult to obtain quantitative error estimates because the sources of error are unknown and the algorithm requires some subjective choice of a “range” (see the appendix).

TABLE 4.3  
The LLE and correlation dimension ( $D_C$ ) for different values of  $\alpha$ , the bifurcation parameter.

$\alpha$	4.85	4.96	4.97	5	5.1
LLE	0	0	$0.004 \pm 2 \cdot 10^{-4}$	$0.018 \pm 3 \cdot 10^{-5}$	$0.032 \pm 8 \cdot 10^{-4}$
$D_C$	$1.000 \pm 3 \cdot 10^{-4}$	$1.002 \pm 2 \cdot 10^{-2}$	$1.67 \pm 7 \cdot 10^{-2}$	$1.87 \pm 3 \cdot 10^{-2}$	$1.91 \pm 2 \cdot 10^{-2}$

A study of the dependence of the LLE on the embedding dimension is presented in the appendix. Although precise error estimates are not available, there is still some value in the predictions made; namely, a clear difference is observed between  $\alpha = 4.96$  and  $\alpha = 4.97$ , which corresponds to the apparent saturation point of the bifurcation diagram presented in Figure 4.7.

**4.4.3. Correlation dimension estimate.** While the Lyapunov exponent measures the rate at which information is lost in a dynamical system, the correlation dimension gives an upper bound on the number of degrees of freedom a system has. This is an important concept for distinguishing deterministic chaos from stochastic chaos. For simple attractors the correlation dimension is an integer, but for strange or chaotic attractors the dimension is fractal. We compute the correlation dimension of our time series using the algorithm presented in [18]. The results for different values of  $\alpha$  are shown in Table 4.3. The magnitude of  $D_C$  is seen to be about 1.9 in the chaotic regime. The implication is that the dynamics of the system is nearly two-dimensional; i.e., a two-dimensional phase space is in principle sufficient to describe the observed

dynamics. Of course, this gives no hint at what that description should be, but the importance of  $D_C$  is in providing an estimate of the degrees of freedom involved.

**5. Conclusions.** A simple model equation consisting of an inviscid Burgers equation forced with a term that depends on the current shock speed is analyzed by calculating its steady-state solutions, the linear stability properties of these solutions, and the nonlinear, time-dependent evolution that starts with the steady state as an initial condition. It is found that the theory and numerical results for the model equation parallel those of the reactive Euler equations of one-dimensional gas dynamics, which have been extensively used to describe detonation waves.

The steady-state theory of the model is analogous to that of the ZND theory of detonation, describing both self-sustained and overdriven solutions. The normal-mode linear stability theory of the model is qualitatively similar to the detonation stability theory, reproducing comparably complex spectral behavior. The nonlinear dynamics, computed with a high-accuracy numerical solver, exhibit the Hopf bifurcation from a stable solution to a limit cycle, together with a subsequent cascade of period-doubling bifurcations, resulting eventually in what is, very likely, chaos. All of these features have their counterparts in the solutions of the reactive Euler equations. The qualitative agreement between the two systems, so drastically different in their complexity, hints at the possibility that a theory for the observed complex dynamics of one-dimensional detonations may be rather simple. Multidimensional detonations are likely to be much more challenging.

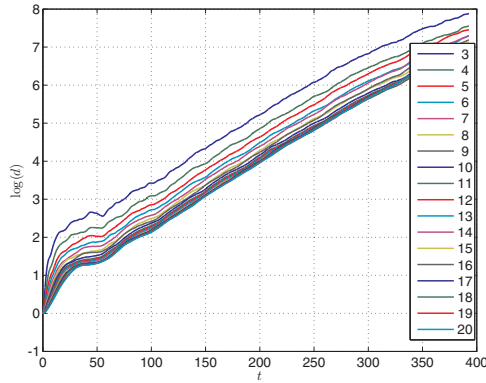
### Appendix. Numerical algorithms.

**A.1. PDE solver.** The hyperbolic system presented in this paper is solved using a method of lines approach, in which we discretize in space and then evolve the resultant ODE system in time. For the spatial discretization, we use a five-point weighted essentially nonoscillatory (WENO) method [38]. Our stencils are biased to the right by one point. As usually done in WENO methods, we introduce a small parameter,  $\epsilon$ , to guarantee that the denominators in the smoothness indicators of the method do not become zero when calculating the weight coefficients. For the problems investigated here, we experimented with  $\epsilon$  between  $10^{-5}$  and  $10^{-10}$ , and the solutions appear to be unaffected by this choice. The chosen  $\epsilon$  for all computations was  $\epsilon = 10^{-6}$ .

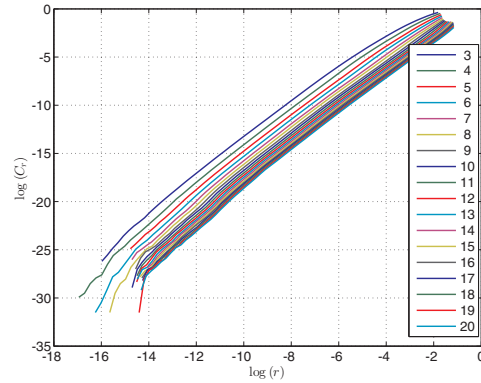
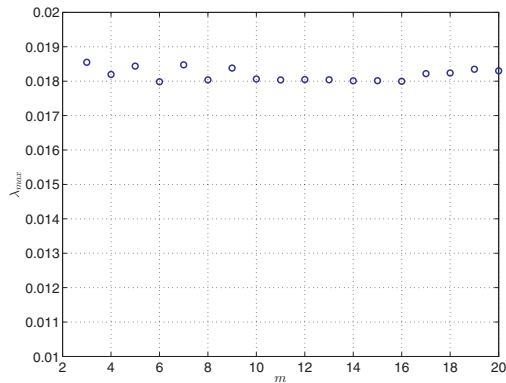
To avoid spurious oscillations, we use a third-order total variation diminishing (TVD) Runge–Kutta time stepping algorithm [17]. Convergence tests were performed using the steady-state solution in the stable regime, for which fifth-order convergence in space was obtained.

**A.2. The LLE.** The algorithm for the LLE consists of the following steps:

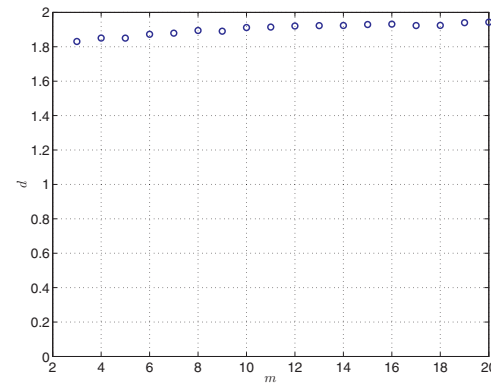
1. Given a time series  $u_s^n$ , embed it in an  $m$ -dimensional space with delay  $\tau$ , as outlined in section 4.4.1.
2. For a given point  $p_i$ , find the closest point  $p_{j_i}$  such that  $|i - j_i| >$  the mean period, where the mean period is estimated by the inverse of the dominant frequency of the power spectrum.
3. Define  $d_i^m(n) = \|p_{i+n} - p_{j_i+n}\|$ . Then,  $d_i(n)$  represents the divergence between trajectories starting at  $p_i$  and  $p_{j_i}$ .
4. Choose  $N$  points randomly on the attractor and compute an average divergence of trajectories by  $d^m(n) = \frac{1}{N} \sum_{i=1}^N d_i^m(n)$ . The number  $N$  is limited either by the amount of available data or by computational restrictions.



(a) The divergence of trajectories for different embedding dimensions.

(b) Plots of  $\log(C_r)$  vs.  $\log(r)$  for different embedding dimensions.

(c) The LLE estimated from (a).



(d) The correlation dimension estimated from (b).

FIG. A.1. Dependence of the LLE and correlation dimension on the choice of the embedding dimension.

5. Plot  $\log(d^m(n))$  versus  $n\Delta t$ .
6. Repeat steps 1–5 for different values of the embedding dimension,  $m$ , and find a region  $t_{\min} < t < t_{\max}$  such that the plot of  $\log(d^m(n))$  versus  $n\Delta t$  is nearly a straight line for the values of  $m$  used.
7. Do a least-squares fit in the region  $t_{\min} < t < t_{\max}$  to extract  $\lambda_1^m$  for each embedding dimension  $m$ .
8. If the values of  $\lambda_1^m$  do not vary much for a wide range of embedding dimensions  $m$ , let  $\lambda_1$  be the average over all embedding dimensions computed.

The algorithm suggested above, which is presented in [33], has some parameters that are not objectively chosen. The value of  $\lambda_1$  depends on, among other things, the choices of  $\tau$ , the range of  $m$  considered, the choices of  $t_{\min}$  and  $t_{\max}$ , and on  $N$ . Of course, it also depends on the quality of the data set and the amount of noise present in it. In [33], a numerical study of this parameter-dependence is performed, and it is claimed that the algorithm is rather robust. In our study, we use the range  $3 \leq m \leq 20$ , fix  $\tau = 150$ , choose  $N = 20,000$ , and choose  $t_{\min}$  and  $t_{\max}$  by looking at the plot of  $\log(d)$  versus  $t$ . A typical plot is shown in Figure A.1, where  $\alpha = 5$ ,  $t_{\min} = 100$ , and  $t_{\max} = 200$ .

In Table A.1, we present the values of the LLE calculated for each given dimension from Figure A.1.

TABLE A.1  
The LLE and the correlation dimension for different embedding dimensions.

$m$	3	4	5	8	10	15	20
LLE	0.0185	0.0182	0.0184	0.0180	0.0181	0.0180	0.0183
$D_C$	1.8306	1.8507	1.8500	1.8904	1.9147	1.9317	1.9432

For other values of  $\alpha$ , the same methodology is applied. The values shown in Table 4.3 are obtained by averaging the LLE over multiple dimensions. The error estimates are the maximum differences between the averages and the entries.

**A.3. Correlation dimension.** The algorithm for computing the correlation dimension follows that of [18]. It consists of the following steps:

1. Given a time series  $u_s^n$ , embed it in an  $m$ -dimensional space with delay  $\tau$ , as outlined in section 4.4.1.
2. Construct a grid  $\bar{r} = (r_1, \dots, r_L)$ , where  $r_1 > \min_{i,j}(\|u_s^i - u_s^j\|)$  and  $r_L < \max_{i,j}(\|u_s^i - u_s^j\|)$ .
3. For each  $r_i$  define the correlation sum, at a given dimension  $m$ , to be  $C^m(r_k) = \frac{1}{N^2} \sum_{i,j=1}^N \theta(r_k - \|u_s^i - u_s^j\|)$ .
4. Plot  $\log(C^m(r_k))$  versus  $\log(r_k)$ .
5. Repeat steps 1–4 for different values of the embedding dimension  $m$ , and find a region  $r_{\min} < r < r_{\max}$  such that the plot of  $\log(C^m(r))$  versus  $\log(r)$  is nearly a straight line for the values of  $m$  used.
6. Do a least-squares fit over the region  $r_{\min} < r < r_{\max}$  to extract  $D_C^m$  for each embedding dimension  $m$ .
7. If the values of  $D_C^m$  do not vary much for a wide range of embedding dimensions  $m$ , let  $D_C$  be the average over all embedding dimensions.

Similar to the LLE calculation, the computed value of  $D_C$  depends on many parameters that cannot be objectively chosen. The choices of  $\tau$ ,  $m$ ,  $r_{\min}$ , and  $r_{\max}$  in particular have an appreciable effect on the value of  $D_C$ . In our study, we use the range  $3 \leq m \leq 20$ , fix  $\tau = 150$ , choose  $N = 5000$ , and choose  $r_{\min}$  and  $r_{\max}$  by looking at the plot of  $\log(C^m(r))$  versus  $\log(r)$ . A typical plot is shown in Figure A.1(a), where  $\alpha = 5$ ,  $\log(r_{\min}) = -8$ , and  $\log(r_{\max}) = -4$ .

In Table A.1, we show the computed values of the correlation dimension for the data presented in Figure A.1(b). Notice that the variability here is much higher than in the computation for the LLE.

#### REFERENCES

- [1] A. BOURLIOUX AND A. J. MAJDA, *Theoretical and numerical structure for unstable two-dimensional detonations*, Combust. Flame, 90 (1992), pp. 211–229.
- [2] J. BUCKMASTER AND J. NEVES, *One-dimensional detonation stability—The spectrum for infinite activation energy*, Phys. Fluids, 31 (1988), pp. 3571–3576.
- [3] P. CLAVIN AND L. HE, *Acoustic effects in the nonlinear oscillations of planar detonations*, Phys. Rev. E, 53 (1996), pp. 4778–4784.
- [4] P. CLAVIN, L. HE, AND F. A. WILLIAMS, *Multidimensional stability analysis of overdriven gaseous detonations*, Phys. Fluids, 9 (1997), pp. 3764–3785.
- [5] P. CLAVIN AND F. A. WILLIAMS, *Analytical studies of the dynamics of gaseous detonations*, Philos. Trans. Roy. Soc. A, 370 (2012), pp. 597–624.
- [6] W. DÖRING, *Über den Detonationvorgang in Gasen*, Ann. Phys., 43 (1943), pp. 421–428.

- [7] J. J. ERPENBECK, *Stability of steady-state equilibrium detonations*, Phys. Fluids, 5 (1962), pp. 604–614.
- [8] J. J. ERPENBECK, *Structure and stability of the square-wave detonation*, in Proceedings of the International Symposium on Combustion, vol. 9, Elsevier, New York, 1963, pp. 442–453.
- [9] W. FICKETT, *Detonation in miniature*, Amer. J. Physics, 47 (1979), pp. 1050–1059.
- [10] W. FICKETT, *Introduction to Detonation Theory*, University of California Press, Berkeley, CA, 1985.
- [11] W. FICKETT, *Stability of the square-wave detonation in a model system*, Phys. D, 16 (1985), pp. 358–370.
- [12] W. FICKETT, *Decay of small planar perturbations on a strong steady detonation: A differential-difference equation for the shock*, Phys. Fluids, 30 (1987), pp. 1299–1309.
- [13] W. FICKETT, *Approach to the steady solution for a plane Chapman–Jouguet detonation*, Phys. Fluids A, 1 (1989), pp. 371–379.
- [14] W. FICKETT AND W. C. DAVIS, *Detonation: Theory and Experiment*, Dover, New York, 2011.
- [15] W. FICKETT AND W. W. WOOD, *Flow calculations for pulsating one-dimensional detonations*, Phys. Fluids, 9 (1966), pp. 903–916.
- [16] A. M. FRASER AND H. L. SWINNEY, *Independent coordinates for strange attractors from mutual information*, Phys. Rev. A, 33 (1986), pp. 1134–1140.
- [17] S. GOTTLIEB AND C.-W. SHU, *Total variation diminishing Runge-Kutta schemes*, Math. Comp., 67 (1998), pp. 73–85.
- [18] P. GRASSBERGER AND I. PROCACCIA, *Measuring the strangeness of strange attractors*, Phys. D, 9 (1983), pp. 189–208.
- [19] L. HE, *On the two-dimensional instability of square-wave detonations*, Combust. Theory Model., 3 (1999), pp. 297–322.
- [20] A. K. HENRICK, T. D. ASLAM, AND J. M. POWERS, *Simulations of pulsating one-dimensional detonations with true fifth order accuracy*, J. Comput. Phys., 213 (2006), pp. 311–329.
- [21] J. HUMPHERYS, G. LYNG, AND K. ZUMBRUN, *Stability of viscous detonations for Majda’s model*, Phys. D, 259 (2013), pp. 63–80.
- [22] A. KASIMOV, L. FARIA, AND R. R. ROSALES, *A model for shock wave chaos*, preprint arXiv:1202.2989, 2012.
- [23] A. R. KASIMOV, L. M. FARIA, AND R. R. ROSALES, *Model for shock wave chaos*, Phys. Rev. Lett., 110 (2013), 104104.
- [24] A. R. KASIMOV AND D. S. STEWART, *On the dynamics of self-sustained one-dimensional detonations: A numerical study in the shock-attached frame*, Phys. Fluids, 16 (2004), pp. 3566–3578.
- [25] H. I. LEE AND D. S. STEWART, *Calculation of linear detonation instability: One-dimensional instability of plane detonation*, J. Fluid Mech., 212 (1990), pp. 103–132.
- [26] J. H. S. LEE, *The Detonation Phenomenon*, Cambridge University Press, Cambridge, UK, 2008.
- [27] A. MAJDA, *A qualitative model for dynamic combustion*, SIAM J. Appl. Math., 41 (1981), pp. 70–93.
- [28] C. MERKWIRTH, U. PARLITZ, I. WEDEKIND, AND W. LAUTERBORN, *TSTOOL Home Page*, University of Göttingen, 2009, <http://www.physik3.gwdg.de/tstool/index.html>.
- [29] H. NG, A. HIGGINS, C. KIYANDA, M. RADULESCU, J. LEE, K. BATES, AND N. NIKIFORAKIS, *Nonlinear dynamics and chaos analysis of one-dimensional pulsating detonations*, Combust. Theory Model, 9 (2005), pp. 159–170.
- [30] E. S. ORAN, J. W. WEBER, JR., E. I. STEFANIW, M. H. LEFEBVRE, AND J. D. ANDERSON, JR., *A numerical study of a two-dimensional  $H_2$ - $O_2$ -Ar detonation using a detailed chemical reaction model*, Combust. Flame, 113 (1998), pp. 147–163.
- [31] M. I. RADULESCU AND J. TANG, *Nonlinear dynamics of self-sustained supersonic reaction waves: Fickett’s detonation analogue*, Phys. Rev. Lett., 107 (2011), 164503.
- [32] R. R. ROSALES AND A. MAJDA, *Weakly nonlinear detonation waves*, SIAM J. Appl. Math., 43 (1983), pp. 1086–1118.
- [33] M. T. ROSENSTEIN, J. J. COLLINS, AND C. J. DE LUCA, *A practical method for calculating largest Lyapunov exponents from small data sets*, Phys. D, 65 (1993), pp. 117–134.
- [34] M. SHORT, *An asymptotic derivation of the linear stability of the square-wave detonation using the Newtonian limit*, Proc. Roy. Soc. London Ser. A, 452 (1996), pp. 2203–2224.
- [35] M. SHORT, *Multidimensional linear stability of a detonation wave at high activation energy*, SIAM J. Appl. Math., 57 (1997), pp. 307–326.
- [36] M. SHORT AND G. J. SHARPE, *Pulsating instability of detonations with a two-step chain-branching reaction model: Theory and numerics*, Combust. Theory Model., 7 (2003), pp. 401–416.



- [37] M. SHORT AND D. S. STEWART, *Cellular detonation stability. Part 1. A normal-mode linear analysis*, J. Fluid Mech., 368 (1998), pp. 229–262.
- [38] C.-W. SHU, *Essentially non-oscillatory and weighted essentially non-oscillatory schemes for hyperbolic conservation laws*, in Advanced Numerical Approximation of Nonlinear Hyperbolic Equations, A. Quarteroni, ed., Lecture Notes in Math. 1697, Springer, Berlin, 1998, pp. 325–432.
- [39] F. TAKENS, *Detecting strange attractors in turbulence*, in Dynamical Systems and Turbulence (Warwick 1980), Springer, New York, 1981, pp. 366–381.
- [40] S. TAKI AND T. FUJIWARA, *Numerical analysis of two-dimensional nonsteady detonations*, AIAA J., 16 (1978), pp. 73–77.
- [41] J. VON NEUMANN, *Theory of Detonation Waves*, Report 549, Office of Scientific Research and Development, National Defense Research Committee Div. B, 1942.
- [42] J. WACKERLE, R. L. RABIE, M. J. GINSBERG, AND A. B. ANDERSON, *Shock Initiation Study of PBX-9404*, technical report, Los Alamos Scientific Lab, Los Alamos, NM, 1978.
- [43] R. M. ZAIDEL, *Stability of detonation waves in gas mixtures*, Dokl. Akad. Nauk SSSR, 136 (1961), pp. 1142–1145.
- [44] Y. B. ZEL'DOVICH, *On the theory of propagation of detonation in gaseous systems*, J. Exp. Theor. Phys., 10 (1940), pp. 542–569.
- [45] F. ZHANG, ED., *Shock Waves Science and Technology Library, Vol. 6: Detonation Dynamics*, Springer, New York, 2012.